JGR Oceans

RESEARCH ARTICLE
10.1029/2023JC019690

The Global Overturning Circulation and the Role of Non-Equilibrium Effects in ECCOv4r4

Tatsu Monkman[1] and **Malte F. Jansen**[1]

[1]The University of Chicago, Chicago, IL, USA

Key Points:

- The meridional overturning circulation (MOC) in Estimating the Circulation and Climate of the Ocean version 4 release 4 (ECCOv4r4) exhibits substantial linkage between the mid-depth and abyssal cells
- Transient isopycnal volume change plays a key role in the watermass budget of the MOC in ECCO
- ECCO's transient interior state must be taken into account when interpreting its climatological state

Correspondence to:

T. Monkman,
tdmonkman@uchicago.edu

Citation:

Monkman, T., & Jansen, M. F. (2024). The global overturning circulation and the role of non-equilibrium effects in ECCOv4r4. *Journal of Geophysical Research: Oceans*, *129*, e2023JC019690. https://doi.org/10.1029/2023JC019690

Received 29 JAN 2023
Accepted 20 DEC 2023

Author Contributions:

Conceptualization: Malte F. Jansen
Data curation: Tatsu Monkman
Formal analysis: Tatsu Monkman, Malte F. Jansen
Funding acquisition: Malte F. Jansen
Investigation: Tatsu Monkman, Malte F. Jansen
Methodology: Tatsu Monkman, Malte F. Jansen
Software: Tatsu Monkman
Visualization: Tatsu Monkman
Writing – original draft: Tatsu Monkman
Writing – review & editing: Tatsu Monkman, Malte F. Jansen

Abstract We quantify the volume transport and watermass transformation rates of the global overturning circulation using the Estimating the Circulation and Climate of the Ocean version 4 release 4 (ECCOv4r4) reanalysis product. The ECCO solution shows large rates of intercell exchange between the mid-depth and abyssal cells, consistent with other recent inferences. About 10 Sv of North Atlantic deep water enters the abyssal cell in the Southern Ocean and is balanced by a similar amount of apparent diapycnal upwelling in the Indo-Pacific. However, much of the upwelling in ECCO's deep ocean is not associated with irreversible watermass transformations, as typically assumed in theoretical models. Instead, a dominant portion of the abyssal circulation in ECCO is associated with isopycnal volume tendencies, reflecting a deep ocean in a state of change and a circulation in which transient tendencies play a leading role in the watermass budget. These volume tendencies are particularly prominent in the Indo-Pacific, where ECCO depicts a cooling and densifying deep ocean with relatively little mixing-driven upwelling, in disagreement with recent observations of deep Indo-Pacific warming trends. Although abyssal ocean observations are insufficient to exclude the trends modeled by ECCO, we note that ECCO's parameterized diapycnal mixing in the abyssal ocean is much smaller than observational studies suggest and may lead to an under-representation of Antarctic Bottom Water consumption in the abyssal ocean. Whether or not ECCO's tendencies are realistic, they are a key part of its abyssal circulation and hence need to be taken into consideration when interpreting the ECCO solution.

Plain Language Summary We analyze results taken from the Estimating the Circulation and Climate of the Ocean (ECCO) state estimate in order to investigate the internal structure and watermass budget of the global ocean's large-scale circulation. The ECCO solution supports the modern view of an interconnected global ocean with substantial exchange between the overturning circulation of the Atlantic and that of the Indo-Pacific via the Southern Ocean. However, our investigation also reveals that the density structure of much of the deep ocean in the ECCO product is in a state of change, and that these changes play a key role in the watermass budget of the circulation. These results reveal disagreement between the model's representation of the deep ocean and the prevailing theoretical depictions of the ocean's large-scale circulation, which generally assume that the circulation is in a steady state. Disagreement between ECCO's deep ocean mixing rates and independent estimates indicate that the trends in ECCO may be biased, but deep ocean observations are insufficient to conclusively infer the true trends.

1. Introduction

The global meridional overturning circulation (MOC) plays a central role in Earth's climate, modulating the exchange of watermasses between the surface and the deep ocean and facilitating a large portion of the world's heat transport and carbon dioxide uptake (Ferrari & Ferreira, 2011; Toggweiler et al., 2006). The MOC is often described in terms of two circulation cells: the mid-depth cell and the abyssal cell. The mid-depth cell is primarily located in the upper- and mid-depths of the Atlantic Ocean and is associated with the formation of North Atlantic Deep Water (NADW) via surface transformations in the north and wind-driven upwelling in the south (Marshall & Speer, 2012). The abyssal cell primarily occupies the deep and abyssal Indo-Pacific basin and is associated with Antarctic Bottom Water (AABW) formation off the coast of Antarctica (Gordon, 2001) and diffusive upwelling in the ocean interior (Weaver et al., 1999). Recent work has shown that these two overturning cells are likely linked via the Southern Ocean (Lumpkin & Speer, 2007; Talley, 2013), where upwelled NADW densifies and enters the abyssal cell as AABW, while upwelled Indo-Pacific water returns to lighter densities and circulates into the upper limb of the mid-depth cell (Talley, 2013). The two overturning cells, plus their exchange in the Southern Ocean, have thus been argued to form a "figure-eight" circulation system (Ferrari et al., 2014).

Despite the importance of the MOC to Earth's past and future climate, our understanding of the MOC's interior structure is incomplete. We still lack a clear consensus on the exchange rate of volume between the mid-depth and abyssal cells, and on the role and rates of diapycnal mixing, which governs the interior watermass transformations thought to be critical to maintaining the MOC. Our incomplete understanding of the structure of the deep ocean circulation, and the associated watermass transformations, leads to uncertainty in predicting its role in future and past climate shifts, and serves as motivation for this study.

Observational and theoretical evidence supports a large amount of exchange between the mid-depth and abyssal cells via the Southern Ocean, although there is some disagreement about the actual magnitude of exchange that occurs. Hydrographic analysis by Talley (2013) suggests that most NADW is converted to abyssal-cell AABW near the coast of Antarctica (≈13 Sv), and recirculates through the abyssal cell before returning into the Atlantic (cf. Ferrari et al., 2014). Inverse analysis by Lumpkin and Speer (2007) shows a somewhat more even partitioning of NADW between the abyssal cell (≈11 Sv) and recirculation within the mid-depth cell (≈7 Sv). A similar partitioning was found by Cessi (2019) in the Estimating the Circulation and Climate of the Ocean version 4 release 2 (ECCOv4r2) state estimate (spanning 1992–2011). A recent study by Rousselet et al. (2021) utilizes ECCOv4r3's climatological mean state to advect Lagrangian drifters along the pathway of NADW in the MOC and finds a similar partition of NADW between "upper" (32%) and "lower" (78%) recirculation routes. Rousselet et al. (2021) argue that the lower route is further partitioned into an abyssal route through the Indo-Pacific (48%) and a "subpolar" cell route (20%) localized to the Southern Ocean. Moreover, Rousselet and Cessi (2022) argue that a portion of NADW densifies and enters the abyssal Indo-Pacific directly at depth, without first upwelling to the surface around Antarctica. The magnitude and structure of the intercell exchange thus remains a subject of debate.

A common assumption, employed in idealized models of the deep ocean overturning circulation (e.g., Gnanadesikan, 1999; Nikurashin & Vallis, 2011; Wolfe & Cessi, 2011), as well as in watermass budget calculations used to infer diapycnal mixing rates (e.g., Ganachaud & Wunsch, 2000; Lumpkin & Speer, 2007; Macdonald et al., 2009; Talley et al., 2003), is that any volume flux convergence below a sub-surface isopycnal is primarily balanced by watermass transformations associated with diapycnal mixing. In this picture, deep water formation in the Northern Hemisphere is balanced by a combination of wind-driven upwelling along isopycnals in the south, which does not require any interior diapycnal watermass transformations, and diapycnal upwelling in the basin interior, which is balanced by mixing-driven watermass transformations. Bottom water formation in the Southern Hemisphere around Antarctica, meanwhile, is assumed to be balanced by mixing-driven upwelling in the basin interiors to the north (de Lavergne et al., 2022; Lumpkin & Speer, 2007; Nikurashin & Vallis, 2011; Talley, 2013). Within this equilibrium framework, any transport balanced by adiabatic isopycnal volume changes due to non-equilibrium temperature and salinity trends are treated as second order with respect to diapycnal mixing. To what degree this advective-diffusive balance holds in the real ocean remains an open question. It is clear that there are tendencies in deep ocean temperatures and salinities as a result of intrinsic variability and climatic changes (e.g., Desbruyères et al., 2017; Gebbie & Huybers, 2019; Messias & Mercier, 2022; Purkey & Johnson, 2010), and trends have also been noted in ECCO (Liang et al., 2017; Wunsch & Heimbach, 2014), but the role of these trends in the MOC and deep ocean watermass budgets has not yet been addressed.

This study investigates the exchange pathways and the watermass transformations that maintain the MOC in ECCO. We focus on the basin-wide volume budgets and hence define inter-cell exchange as the amount of NADW that leaves the Atlantic below the isopycnal that separates the mid-depth and abyssal cells in the Southern Ocean, which must be balanced by a similar amount of upwelling in the Indo-Pacific (Nadeau et al., 2019). This quantity measures the net exchange of volume between the overturning cells and basins, although it does not reveal the pathways taken by individual water parcels (for which readers should refer to Rousselet et al. (2021) and Rousselet and Cessi (2022)). In each basin, we then apply an isopycnal volume budget decomposition based on Walin (1982) (see also Lee et al. (2002), Megann (2017), Newsom et al. (2016) and Urakawa and Hasumi (2014)) which allows us to decompose any net up- or down-welling into specific watermass transformation processes. In addition to the transport associated with explicit diapycnal mixing, we calculate the transport associated with numerical mixing, geothermal heating, and isopycnal volume tendencies, that is, balanced by trends in abyssal temperature and salinity. By presenting a complete water mass budget decomposition of ECCO's deep and abyssal overturning circulation, we hope to give a more complete picture of the processes governing the MOC in ECCO.

Our results generally support the interconnected view of the MOC, with a large amount of exchange between the mid-depth and abyssal cells, roughly in line with existing theory and observations. However, the watermass

budget shows that ECCO's deep ocean is not in equilibrium and that isopycnal volume changes associated with trends in the deep ocean density play a major role in ECCO's deep ocean watermass budgets.

2. Methods

2.1. The ECCOv4r4 State Estimate

We analyze monthly mean results taken from the ECCOv4r4 ocean state estimate (ECCO Consortium et al., 2021, 2022; Forget et al., 2015). The ECCO setup comprises a non-linear inverse modeling framework utilizing MITgcm (Marshall et al., 1997) in conjunction with the adjoint method (Forget & Ponte, 2015) to produce an optimized solution of the hydrostatic Boussinesq equations fit to a suite of oceanographic data spanning a 26-year time period from 1992 to 2017 (ECCO Consortium et al., 2021). The model component of ECCOv4r4 uses the Lat-Lon-Cap 90 (LLC90) grid with a latitudinally varying horizontal resolution between approximately 20–40 km at 80°N/S to 110 km at 10°N/S. Further details about the ECCO state estimate are provided in Forget et al. (2015) and ECCO Consortium et al. (2021).

2.2. The Meridional Overturning Circulation in Potential Density Coordinates

In order to evaluate the overall volume budgets of the global ocean circulation we employ the isopycnal streamfunction, $\Psi(y, \sigma_2)$, as a function of latitude (y) and potential density referenced to 2000 dbar (σ_2). We choose σ_2 because it corresponds to the approximate average local pressure of NADW within the Atlantic interior and has been used previously by Rousselet et al. (2021) and Rousselet and Cessi (2022). $\Psi(y, \sigma_2)$ is defined as the zonally and vertically integrated sum of the resolved meridional transport field, $\mathbf{v}(x, y, z, t)$, and the parameterized meridional eddy transport, $\mathbf{v}^*(x, y, z, t)$, from the ocean bottom to a given σ_2 surface. Since the ECCO fields are given in z-space, we begin our analysis by calculating the local streamfunction, $\psi(x, y, \sigma_2, t)$, by vertically integrating the transport to a vertical σ_2 grid:

$$\psi(x, y, \sigma_2, t) = \int_{-H(x,y)}^{z(x,y,\sigma_2,t)} \mathbf{v}(x, y, z, t) + \mathbf{v}^*(x, y, z, t) dz, \tag{1}$$

where $H(x, y)$ denotes the ocean depth and $z(x, y, \sigma_2, t)$ gives the depth of an isopycnal surface σ_2 at a particular location, found by linearly interpolating σ_2 between vertical grid points. The vertical integral in Equation 1 is performed on the native model grid, before linearly interpolating ψ to the height of a given isopycnal $z(x, y, \sigma_2, t)$. (This technique is similar to Ferrari and Ferreira (2011) and perfectly preserves the meridional mass transport in each column. To test the sensitivity of our results to the interpolation method we repeated our analysis without any interpolation (i.e., the integral in Equation 1 simply includes all gridboxes with potential density smaller than the specified σ_2 level, which amounts to assuming a piece-wise constant rather than piece-wise linear density profile). Differences between the two methods were found to be on the order of 1% and hence do not affect our conclusions). Next, we integrate $\psi(x, y, \sigma_2, t)$ in the zonal and take the time average:

$$\Psi(y, \sigma_2) = \overline{\int_{x_0(y)}^{x_1(y)} \psi(x, y, \sigma_2, t) dx}, \tag{2}$$

where $\int_{x_0(y)}^{x_1(y)} dx$ gives the zonal integral at a given latitude y across an ocean basin bounded by longitudes x_0 and x_1, and $\overline{(\cdot)}$ denotes the time-average of the enclosed quantity over the full ECCO time period. We calculate $\Psi(y, \sigma_2)$ across three ocean basins: the Atlantic (In order to remove contributions from the North Sea circulation to the AMOC streamfunction we exclude regions East of the Greenland-Iceland-Scotland (GIS) ridge system from our Atlantic mask (Figure 1). Notice that all isopycnals either out-crop into the surface layer or in-crop into the seafloor before reaching the open boundary at the GIS ridge system. As a result the overflows do not affect the interior volume budgets presented in Section 2.3), Southern, and Indo-Pacific Oceans, which in turn are divided by the continents and the 32°S parallel (Figure 1).

2.3. Volume Budget Decomposition in the Interior

We employ an isopycnal volume-budget analysis based on Walin (1982) and Newsom et al. (2016) to diagnose the processes that balance diapycnal advection within the large-scale circulation in ECCOv4r4 (Figure 2). We

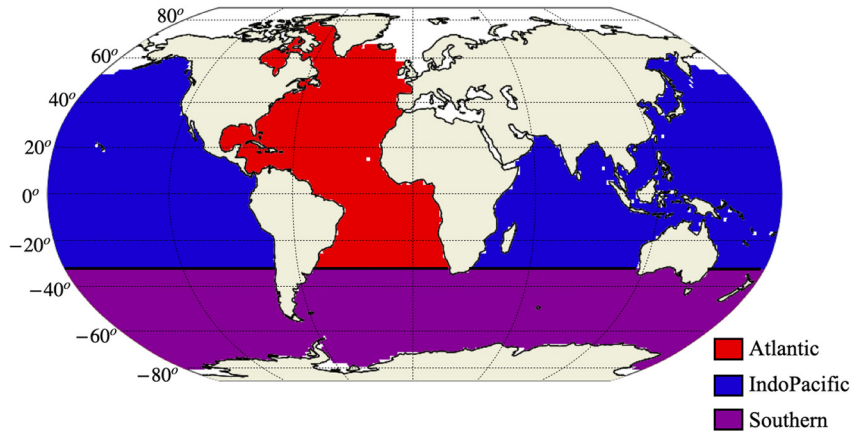

Figure 1. Basin masks used for subdividing the global ocean. The Atlantic basin (red) extends from 32°S into the Labrador and Baffin seas in the north. The Indo-Pacific basins (blue) are considered together and extend from 32°S to the Aleutians in the north. The Southern Ocean (purple) is bounded in the north at 32°S and extends to the coast of Antarctica. Note that the basin masks shown here do not include the poleward limits of the interior volumes considered in Section 3 that are imposed by the outcrops of isopycnal surfaces into the surface layer, whose locations vary depending on the density surface under consideration.

consider the volume flux balance of a volume of ocean, $V(y_1, y_2, \sigma_2)$, bounded above by an isopycnal of density σ_2, in the zonal direction by continental boundaries, and in the meridional by the latitudes y_1 in the south and y_2 in the north. We define the bottom of the surface layer as the maximum surface potential density at or equatorwards of any given latitude over the zonal width of the basin and the entire ECCO time period (i.e., the bottom

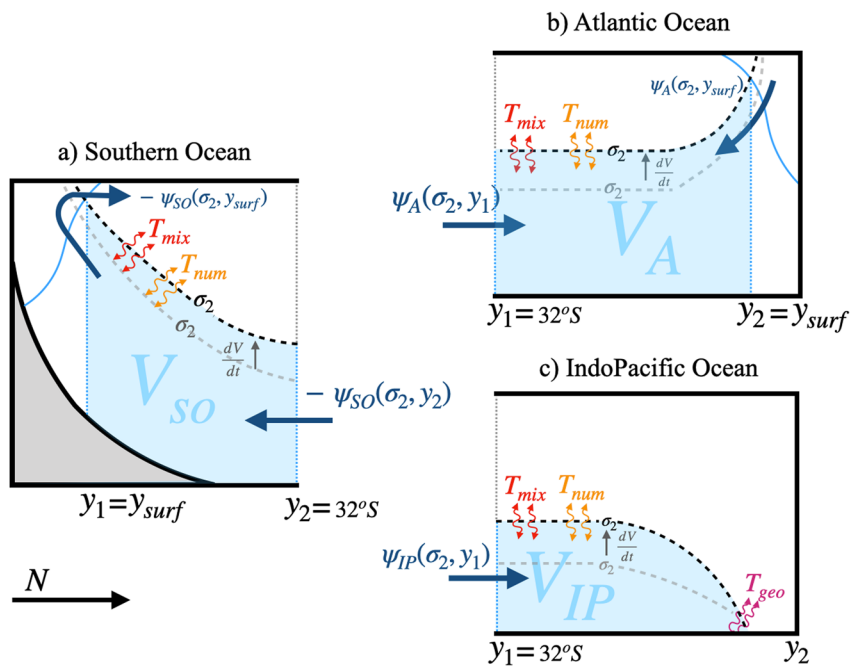

Figure 2. Schematic of the water-mass-transformation framework used in this study, applied to the Atlantic (subscript A), Indo-Pacific (subscript IP), and Southern Ocean (subscript SO). Black dashed lines indicate an isopycnal surface of density σ_2. Transports into and out of isopycnal volumes are indicated by arrows, with dark blue indicating net advective flux ($\Psi(y, \sigma_2)$), red the transport balanced by explicit diapycnal diffusion (T_{mix}), orange the transport balanced by numerical diffusion (T_{num}), purple transport balancing geothermal heating (T_{geo}), and gray apparent diapycnal transport balanced by volume change (dV/dt). Latitudes defining the southern and northern meridional bounds of the ocean basins are given by dotted blue lines and labeled y_1 and y_2, respectively, and the latitude where the isopycnal intersects with the surface layer is given by y_{surf}. The bottom of the surface layer is indicated by solid blue lines.

of the surface layer, and with it the outcrop latitude, does not depend on time or longitude). Following volume conservation, the total meridional transport in and out of the volume below any given isopycnal can be expressed as the sum of the volume tendency and various watermass transformation proccesses at the bounding isopycnal:

$$\begin{aligned}\Delta\Psi = &\overline{\frac{d}{dt}V(y_1, y_2, \sigma_2, t)} + \overline{T_{geo}(y_1, y_2, \sigma_2, t)} + \overline{T_{plume}(y_1, y_2, \sigma_2, t)} \\ &+ \overline{T_{mix}(y_1, y_2, \sigma_2, t)} + \overline{T_{num}(y_1, y_2, \sigma_2, t)} + \overline{R(y_1, y_2, \sigma_2, t)}.\end{aligned} \tag{3}$$

Here $\Delta\Psi = \Psi(y_2, \sigma_2) - \Psi(y_1, \sigma_2)$ is the net transport across the northern and southern boundaries which must, by volume conservation, be balanced by the terms on the RHS (see also Figure 2).

$\overline{\frac{d}{dt}V(y_1, y_2, \sigma_2, t)}$ is the time-averaged change in the total volume itself resulting from any net volume convergence below a given isopycnal:

$$\frac{d}{dt}V(y_1, y_2, \sigma_2, t) = \frac{d}{dt}\iint_{A_{\sigma_2}(y_1, y_2)} h(x, y, \sigma_2, t)\, dA, \tag{4}$$

where $h(x, y, \sigma_2, t) = z(x, y, \sigma_2, t) + H(x, y)$ is the height of the isopycnal above the ocean bottom and $A_{\sigma_2}(y_1, y_2)$ is the basin area bounded in the south and north by y_1 and y_2, respectively.

$T_{geo}(y_1, y_2, \sigma_2, t)$ is the diapycnal transport balanced by geothermal heating:

$$T_{geo}(y_1, y_2, \sigma_2, t) = -\frac{\partial}{\partial\sigma_2}\iint_{A_I(y_1, y_2, \sigma_2, t)} \frac{\alpha Q_{geo}(x, y)}{c_p} dA, \tag{5}$$

where $A_I(y_1, y_2, \sigma_2, t)$ is the area where the bottom density $\sigma_{2bottom} \geq \sigma_2$ within the domain bounded by y_1, y_2 and the sides of the basin, $Q_{geo}(x, y)$ is the geothermal heat flux at the ocean floor, $\alpha = -\frac{1}{\sigma_2}\frac{\partial\sigma_2}{\partial\theta}$ is the thermal expansion coefficient, and c_p is the heat capacity of seawater (see de Lavergne et al. (2016) for a full derivation). The integral in Equation 5 is computed on the model grid over small σ_2 bins following Abernathey et al. (2016, SI (S11)).

T_{plume} gives the buoyancy forcing contribution due to salt plume forcing (a parameterized in-situ forcing in ECCO), and is computed as

$$T_{plume}(y_1, y_2, \sigma_2, t) = \frac{\partial}{\partial\sigma_2}\iiint_{V(y_1, y_2, \sigma_2, t)} \frac{\partial\sigma_2}{\partial S}\dot{S}_{plume}(y_1, y_2, \sigma_2, t) dV, \tag{6}$$

where $\dot{S}_{plume}$ is the salinity tendency (psu/s) due to in-situ salt plume flux, and is only significant in the Southern Ocean. The integral above is again taken on the model grid before interpolating to σ_2 levels.

$T_{mix}(y_1, y_2, \sigma_2, t)$ represents the watermass transformation rate due to explicitly parameterized diapycnal mixing (In addition to explicitly parameterized background vertical diffusion, which is optimized as part of the ECCO inversion, T_{mix} contains mixing contributions from parameterized mixing due to the Gaspar, Gregoris, and Lefevre (GGL) scheme (Gaspar et al., 1990), isoneutral mixing when the local neutral slope is not aligned with the slope of the σ_2 surface, and horizontal mixing in the presence of slope-clipping along steep isopycnals. (The MITgcm configuration used for ECCO employs a slope clipping that limits the effective isopycnal slope used in the Gent and Mcwilliams (1990) and Redi (1982) parameterizations to a maximum value of $2 \cdot 10^{-3}$. When this maximum slope is exceeded, mixing is no longer isoneutral.) All of these terms contribute to diapycnal mixing but their individual contributions are difficult to diagnose explicitly) in ECCO, which we derive from the diffusive tendencies of temperature and salinity:

$$T_{mix}(y_1, y_2, \sigma_2, t) = \frac{\partial}{\partial\sigma_2}\iiint_{V(y_1, y_2, \sigma_2, t)} \frac{\partial\sigma_2}{\partial\theta}\dot{\theta}_{mix}(x, z, y, t) + \frac{\partial\sigma_2}{\partial S}\dot{S}_{mix}(x, z, y, t) dV, \tag{7}$$

where $\dot{\theta}_{mix}(x, z, y, t)$ and $\dot{S}_{mix}(x, z, y, t)$ are the temperature and salinity tendencies due to diffusive flux convergence, respectively. $\dot{\theta}_{mix}(x, z, y, t)$ and $\dot{S}_{mix}(x, z, y, t)$ can be computed exactly based on ECCO diagnostics, as discussed in Piecuch (2017). As in Equations 1 and 6 the vertical integral is taken on the model grid before interpolating to σ_2 levels.

Additionally, we must take into account the effects of numerical diffusion associated with inaccuracies in ECCO's advection scheme, T_{num}. Numerical diffusion is an inherent property of z-space ocean models such as ECCO,

and can reach comparable magnitude to explicit mixing (Griffies et al. (2000), Lee et al. (2002)). Previous studies have estimated numerical diffusion simply as the residual of the volume budget described above (Lee et al. (2002); Megann (2017); Urakawa and Hasumi (2014)). Here, we take a slightly more direct path and characterize the contribution from numerical diffusion as the residual between the advective flux derived from the diagnosed density tendency due to the advection scheme and the flux implied by the net volume transport across the volume's horizontal boundaries, $\Delta\Psi$:

$$T_{num}(y_1, y_2, \sigma_2, t) = \Delta\Psi + \frac{\partial}{\partial\sigma} \iiint_{V(y_1, y_2, \sigma_2, t)} \frac{\partial\sigma_2}{\partial\theta}\dot{\theta}_{adv}(x, z, y, t) + \frac{\partial\sigma_2}{\partial S}\dot{S}_{adv}(x, z, y, t)dV, \tag{8}$$

where $\dot{\theta}_{adv}(x, z, y, t)$ and $\dot{S}_{adv}(x, z, y, t)$ are the temperature and salinity tendencies due to the advection scheme, which can be calculated from the ECCO diagnostics (Piecuch, 2017), and include any numerical diffusion arising from the discretization (See the Appendix A for further details). This approach is particularly suited to ECCO, where the θ and S budgets can be closed exactly.

The final term in Equation 3, $R(y_1, y_2, \sigma_2, t)$, is the residual and reflects inaccuracies in our volume budget computation. By applying Equation 3 to specific domains of interest, we can estimate the major drivers of interior water-mass transformations that balance any net up- or down-welling across the different basins. It should be noted that an additional contribution from shortwave penetrating flux is included in the ECCO model and can in theory have an effect below the surface layer, as defined here, but was found to be negligible in our budget.

We can further decompose the isopycnal volume tendency itself to determine the individual contributions from changes in the temperature and salinity of the deep ocean:

$$\overline{\frac{d}{dt}V(y_1, y_2, \sigma_2, t)} = -\overline{T_\Theta(y_1, y_2, \sigma_2, t)} - \overline{T_S(y_1, y_2, \sigma_2, t)} - \overline{R(y_1, y_2, \sigma_2, t)}, \tag{9}$$

where $-T_\Theta(y_1, y_2, \sigma_2, t)$, $-T_S(y_1, y_2, \sigma_2, t)$ are the individual volume tendencies due to the temperature- and salinity-driven buoyancy tendencies, respectively:

$$\begin{aligned} T_\Theta(x, y, z, t) &= \frac{\partial}{\partial\sigma} \iiint_{V_{\sigma_2}} \frac{\partial\sigma}{\partial\theta}\dot{\theta}(x, y, z, t)dV \\ T_S(x, y, z, t) &= \frac{\partial}{\partial\sigma} \iiint_{V_{\sigma_2}} \frac{\partial\sigma}{\partial S}\dot{S}(x, y, z, t)dV. \end{aligned} \tag{10}$$

As previously, the term $R(y_1, y_2, \sigma_2, t)$ in Equation 9 is the residual due to any disagreement between the volume tendency we infer directly from Equation 4 and indirectly from the density tendencies in Equation 9. Because the temperature and salinity budgets in ECCO can be closed exactly, it can be shown that $R(y_1, y_2, \sigma_2, t)$ in Equation 9 is the same as $R(y_1, y_2, \sigma_2, t)$ in Equation 3. Here we find that $R(y_1, y_2, \sigma_2, t)$ is generally small.

3. Results

3.1. The Isopycanl Overturning in ECCO

The isopycnal overturning in ECCOv4r4 (Figure 3) is in broad agreement with that derived in other studies (e.g., Cessi, 2019; Lumpkin & Speer, 2007) and the magnitudes of the overturning cells generally fall within uncertainties established by observation-based estimates (Lumpkin and Speer (2007); Talley (2013); Kunze (2017)), as previously found for ECCOv4r2 by Cessi (2019). The mid-depth cell occupies the Atlantic with a peak overturning strength of 17.2 Sv occurring at 55^{o}N, in good agreement with other estimates (Lumpkin & Speer, 2007; Talley, 2013). The abyssal cell dominates the Indo-Pacific and the lower part of the Southern Ocean and peaks at approximately 14.4 Sv at 36°S, a substantially weaker value than that derived by Lumpkin and Speer (2007) (20 Sv), Talley (2013) (29 Sv), and Kunze (2017) (20 Sv), but similar to the estimates of de Lavergne et al. (2016) (10–15 Sv). The abyssal cell in our analysis is also weaker than the global maximum value reported in Cessi (2019) (20 Sv) for ECCO version 4 release 2.

The net exchange of volume between the Atlantic's mid-depth cell and the abyssal cell can be found by considering the overlap between the Atlantic, Indo-Pacific and Southern Ocean overturning stream functions at 32°S

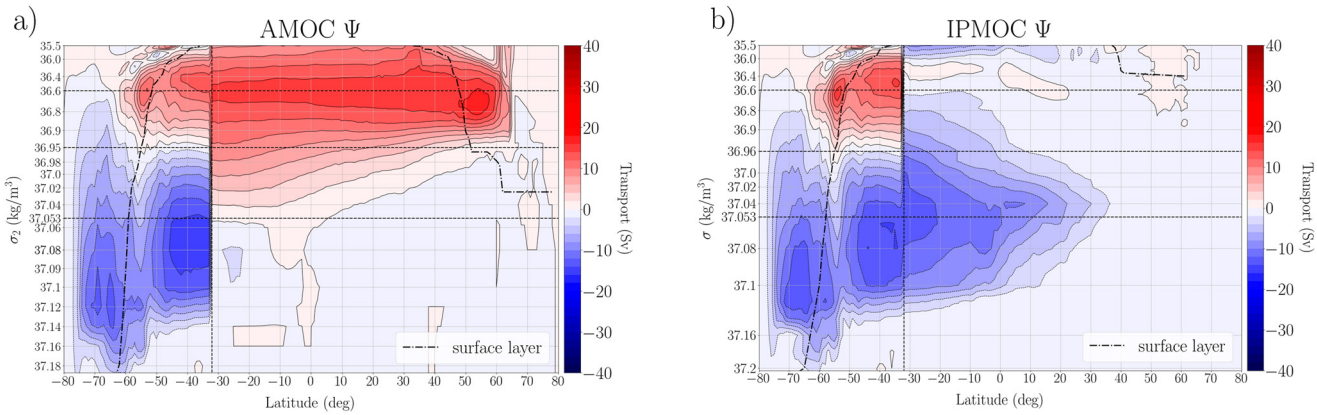

Figure 3. Atlantic, Indo-Pacific, and Southern Ocean stream functions in potential density space (referenced to 2000 dbar), calculated from Estimating the Circulation and Climate of the Ocean version 4 release 4 (ECCOv4r4) and averaged over the full ECCO time period (1992–2017). (a) Atlantic Meridional Overturning Circulation (AMOC) and (b) Indo-Pacific Meridional Overturning Circulation. The Southern Ocean Meridional Overturning Circulation is plotted in both (a) and (b) south of 32°S. Positive (red) denotes clockwise flow and negative (blue) denotes counterclockwise flow (CL = 2 Sv). The dash-dotted line indicates the bottom of the surface layer (see text). The vertical dashed line indicates the northern end of the Southern Ocean at 32°S. Horizontal dashed lines denote specific density surfaces of interest: the upper bound of southward-flowing North Atlantic Deep Water (NADW) entering the Southern Ocean: $\sigma_2 = 1036.6$ kg/m^3, the division between the mid-depth and lower cells in the Southern Ocean: $\sigma_2 = 1036.95$ kg/m^3, and the maximum density of NADW entering the Southern Ocean: $\sigma_2 = 1037.053$ kg/m^3. The density-axis is stretched to reflect the average isopycnal depth within the Atlantic for $\sigma_2 < 1037.1$ kg/m^3 (the maximum density in the Atlantic) and is extended linearly to the highest densities in the Southern Ocean. The same density axis is used in subsequent plots. Note that the AMOC stream function is not well defined north of 60N and above $\sigma_2 \approx 1036.9$ kg/m^3 due to open zonal boundaries along the Greenland-Iceland-Scotland ridge system.

(cf. Nadeau et al., 2019). In ECCOv4r4, 14.2 Sv of NADW exit the Atlantic at 32°S, of which 4.6 Sv enter the Southern Ocean at density classes occupied by the mid-depth cell ($\sigma_2 < 1036.95$ kg/m^3), while 9.6 Sv of NADW enter the Southern Ocean in the density range of the abyssal cell ($\sigma_2 \geq 1036.95$ kg/m^3) and hence must be balanced by a similar amount of upwelling in the Indo-Pacific. Large-scale diapycnal transport is visible beneath the surface layer in all ocean basins (Figures 3 and 4). In the Atlantic, ≈1.2 Sv of NADW upwells diabatically at $\sigma_2 = 1036.6$ kg/m^3 and returns to the surface within the North Atlantic. Denser NADW downwells over the length of the Atlantic yielding around 8.1 Sv of downwelling at $\sigma_2 = 1036.95$ kg/m^3 (Figure 3a). The Indo-Pacific, meanwhile, is dominated by the abyssal cell with an upwelling of 14.4 Sv at $\sigma_2 = 1037.053$ kg/m^3. Of the abyssal circulation that returns to the Southern Ocean, 4.8 Sv enter at densities below $\sigma_2 = 1036.95$ kg/m^3 and recirculate through the abyssal cell while the remaining 9.6 Sv return in the buoyancy range of the mid-depth cell, balancing the transfer of NADW into the abyssal cell.

3.2. Volume Budget and Watermass Transformations

We now examine the isopycnal volume budgets in the Atlantic, Indo-Pacific, and Southern Ocean interiors in order to identify the watermass transformation processes associated with the deep ocean circulation. As above, we primarily focus on the net transformations across the isopycnals $\sigma_2 = 1036.6$ kg/m^3 (marking the maximum of the mid-depth cell in the South Atlantic), $\sigma_2 = 1036.95$ kg/m^3 (marking the division between the mid-depth and abyssal cell at 32°S), and $\sigma_2 = 1037.053$ kg/m^3 (marking the bottom of NADW in the South Atlantic as well as the maximum of the abyssal cell in the Indo-Pacific). We find that volume tendency plays a leading role in driving diabatic watermass transformations across these isopycnals in all basins, while, surprisingly, explicit mixing-driven upwelling is relatively small in both the deep Atlantic and Indo-Pacific.

In the Atlantic, we see a small net upwelling signal at $\sigma_2 = 1036.6$ kg/m^3 (1.2 Sv) which is primarily due to numerical diffusion (2.2 Sv), partially compensated by explicit mixing (−0.9 Sv) and volume tendency (−0.2 Sv). Deeper in the Atlantic, the diapycnal downwelling of NADW at $\sigma_2 = 1036.95$ kg/m^3 (−8.1 Sv) is associated primarily with the volume tendency term, dV/dt (−5.5 Sv), with a smaller contribution associated with numerical diffusion (−2.6 Sv). Net diabatic transformations in the Atlantic at $\sigma_2 = 1037.053$ kg/m^3, meanwhile, are quite small (−0.73 Sv) with a compensation between a negative volume tendency signal (−3.6 Sv) and small positive contributions from numerical diffusion (0.9 Sv), explicit mixing (1.0 Sv), and geothermal heating (0.7 Sv).

In the Indo-Pacific, the volume tendency contribution again dominates, particularly over the depth range of the abyssal cell. The upper Indo-Pacific contains only a small amount of net transport (2.0 Sv) at the $\sigma_2 = 1036.6$ kg/m^3

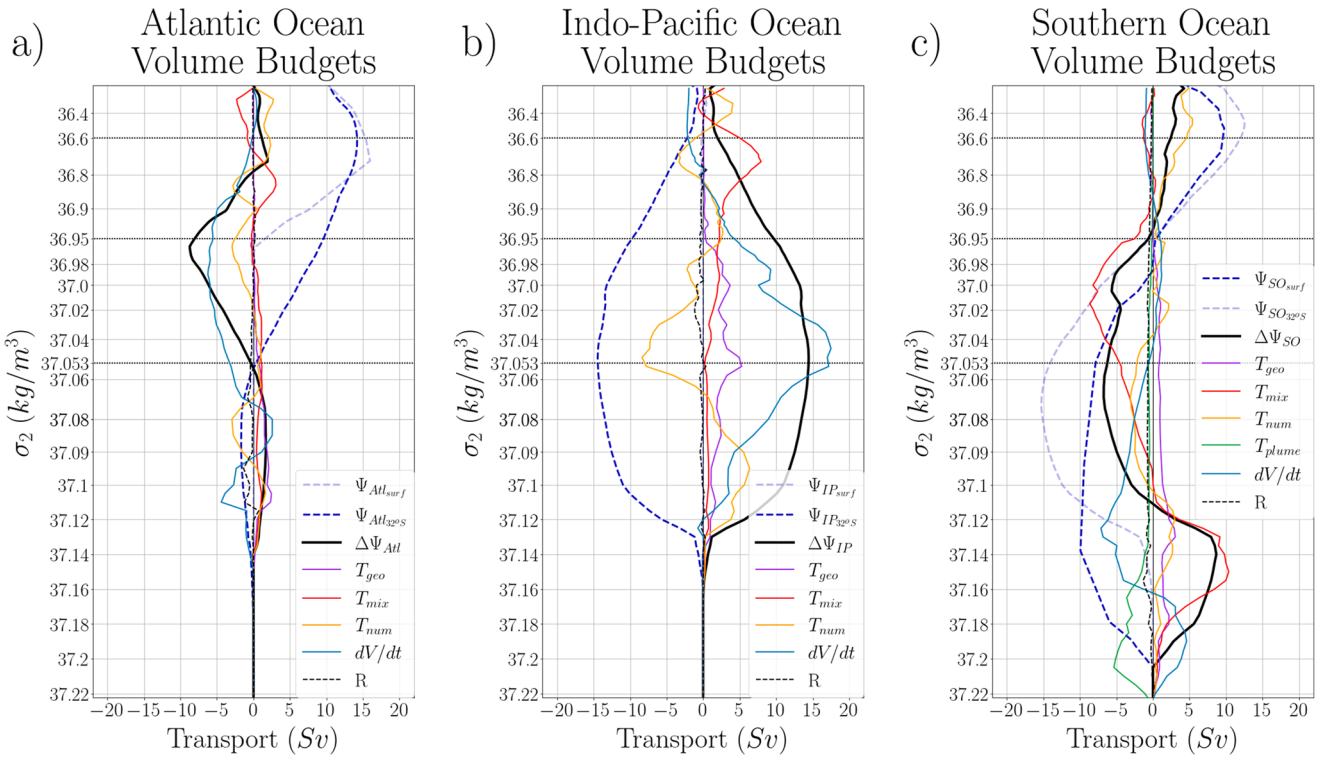

Figure 4. Volume budget decompositions over the Atlantic Ocean (a), Indo-Pacific Ocean (b), and Southern Ocean (c). Solid black lines denote net diapycnal transport at each density surface, inferred from the difference between Ψ across each region's northern (dashed light blue) and southern (dashed dark blue) boundaries. The subscript *Surf* refers to the stream function at the bottom of the surface layer, defined by the minimum surface density at a given latitude (Figure 2). The net diapycnal transport (solid black) is decomposed into contributions from: geothermal transformations (T_{geo}, solid purple), explicit mixing (T_{mix}, solid red), numerical diffusion (T_{num}, solid orange), isopycnal volume change (dV/dt, solid cyan), and salt plume flux forcing (T_{plume}, solid green) which is only significant in the Southern Ocean. *R* (dashed black) gives the residual.

isopycnal, where the effect of explicit mixing (5.0 Sv) is largely balanced by volume tendency (−2.1 Sv) and numerical diffusion (−1.1 Sv). Indo-Pacific upwelling at σ_2 = 1036.95 kg/m^3 is much larger (9.7 Sv), and is primarily associated with a volume tendency (4.3 Sv), with additional contributions from numerical diffusion (2.5 Sv) and explicit mixing (2.2 Sv) and a small contribution from geothermal heating (0.8 Sv). Diapycnal upwelling in the Pacific peaks near σ_2 = 1037.053 kg/m^3 where it reaches 14.5 Sv. This upwelling is primarily balanced by the volume tendency term, contributing 17.0 Sv, with a smaller contribution from geothermal heating (3.3 Sv), and substantial compensation associated with numerical diffusion (−8.4 Sv). Numerical diffusion also plays a large role in the densest regions of the Indo-Pacific, peaking at 6.4 Sv at around σ_2 = 1037.053 kg/m^3.

In the Southern Ocean, volume tendency, numerical diffusion, and explicit mixing all play major roles. Upwelling at σ_2 = 1036.6 kg/m^3 in the interior Southern Ocean (2.4 Sv) is associated with numerical diffusion (4.6 Sv), with compensating contributions from explicit mixing (−1.3 Sv) and volume tendency (−1.0 Sv). Interior transformations across σ_2 = 1036.95 kg/m^3 are small. Transformations at the σ_2 = 1037.053 kg/m^3 isopycnal in the Southern Ocean yield a net interior downwelling of −6.2 Sv which is primarily driven by explicit mixing (−4.9 Sv). It should be noted as well that a large amount of mixing-driven up- and down-welling is present in the abyssal Southern Ocean and is likely related to slope-clipping along steep isopycnals in the isopycnal mixing scheme (In ECCO's representation of the Southern Ocean isopycnal slopes frequently exceed the model's slope clipping threshold of $4 \cdot 10^{-3}(kg/m^3)/m$. See also Footnote 3). Transformations due to salt plume forcing are also prevalent in the densest regions of Southern Ocean, contributing −5.4 Sv at the σ_2 = 1037.205 kg/m^3 isopycnal, and are primarily balanced by a volume tendency.

3.3. Volume Tendency Decomposition

The importance of the *dV/dt* terms that we observe in ECCO's overturning circulation merits further discussion. These volume tendencies are associated with density trends, which in turn can be decomposed into temperature

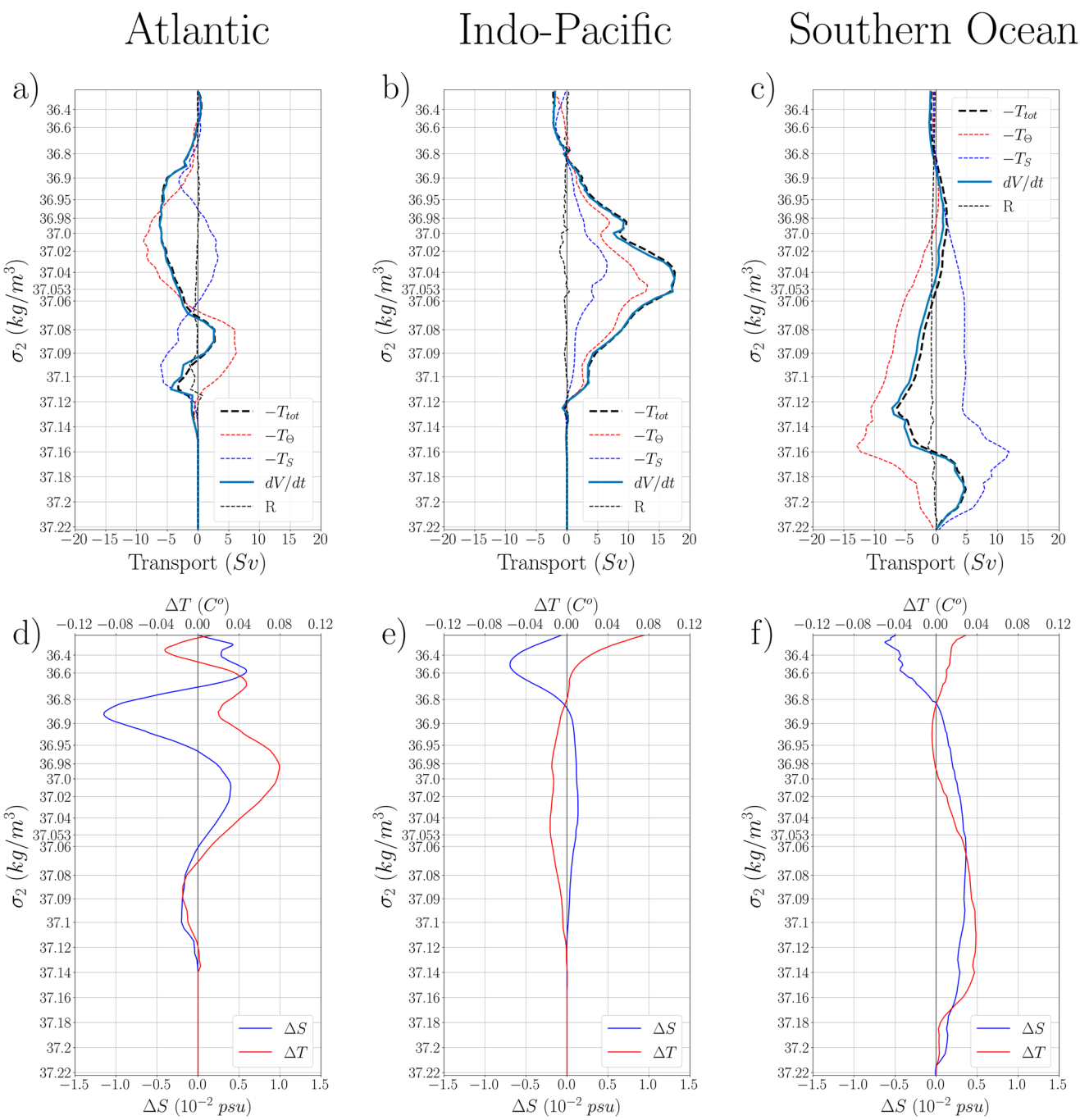

Figure 5. Volume tendency decompositions and net temperature and salinity changes over the Estimating the Circulation and Climate of the Ocean (ECCO) time period (1992–2017) across the Atlantic Ocean (a and d), Indo-Pacific Ocean (b and e), and Southern Ocean (c and f). In (a–c), total isopycnal volume change (solid cyan, Figure 4) across each basin is shown together with the estimated volume change from the total buoyancy tendency, $-T_{tot} = -T_\Theta - T_S$ (cf. Equation 9, bold dashed black), and its temperature and salinity components, $-T_\Theta$ and $-T_S$ (thin dashed red and thin dashed blue, respectively). Panels (d–f) show the corresponding basin-averaged temperature (ΔT, red) and salinity (ΔS, blue) changes over the 26-year ECCO time period.

and salinity trends. The decomposition of the isopycnal volume tendencies into contributions from temperature and salinity trends, together with the associated temperature and salinity trends themselves are shown in Figure 5.

In the Atlantic, the most notable feature of the volume tendency is a strong isopycnal deepening in the depth range of the lower limb of the AMOC between σ_2 = 1036.6 kg/m^3 and σ_2 = 1037.07 kg/m^3, which is associated with a basin-averaged warming of 0.08^oC over the 24-year ECCO time period. The Atlantic also exhibits

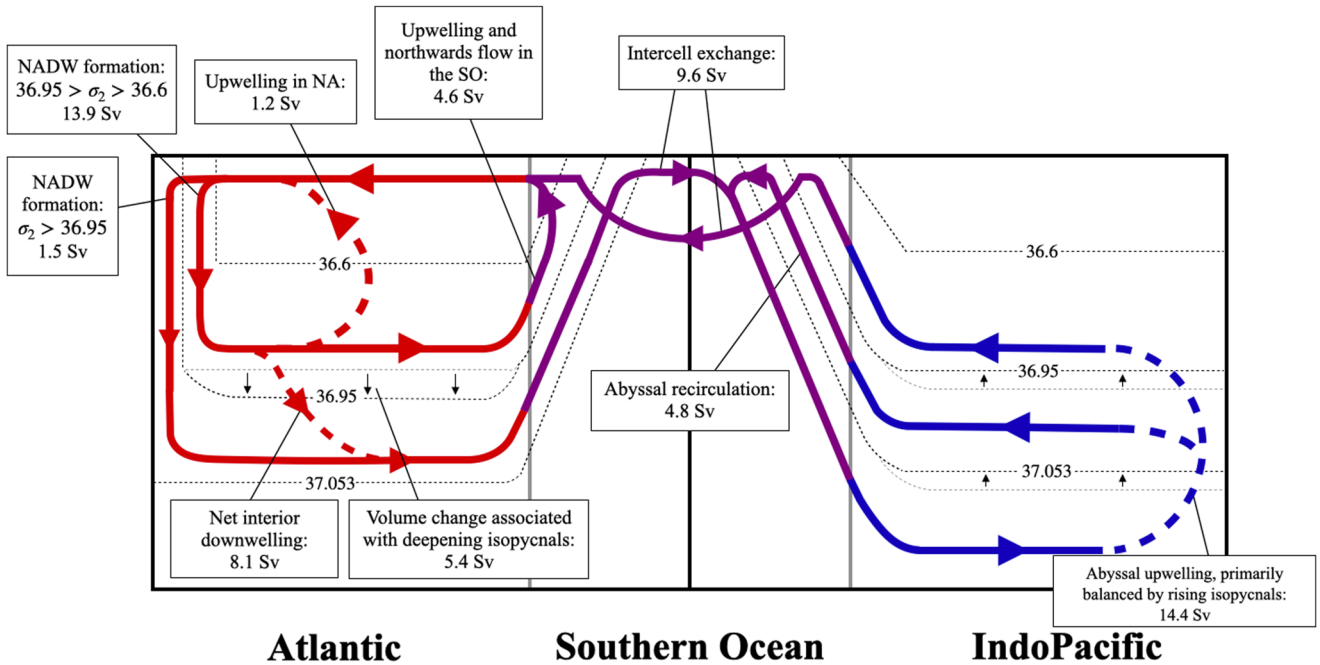

Figure 6. Schematic representation of the overturning, inferred from the stream function and volume budget decomposition (Figures 3 and 4). Net transport within the Atlantic Ocean (red arrows), Southern Ocean (purple arrows), and Indo-Pacific Ocean (blue arrows), are shown. Arrows denote direction of flow. Solid and dashed arrows below the surface denote primarily along- and across-isopycnal pathways, respectively. Dashed black lines denote the specific densities discussed in Figure 3, and isopycnal depth changes are indicated where they are the dominant contributor balancing up- and down-welling.

a small amount of cooling in the lower density ranges of the abyssal ocean, amounting to −0.002 C° over the ECCO period, although this trend is partially compensated by a salinity-driven lightening that dominates below $\sigma_2 = 1037.09$ kg/m^3.

In the Indo-Pacific, cooling plays the leading role in the isopycnal shoaling between $\sigma_2 = 1036.8$ kg/m^3 and $\sigma_2 = 1037.12$ kg/m^3, the main density range of the abyssal cell. Here, a basin-averaged cooling of about 0.016 C° occurs over the ECCO period and accounts for −13.1 Sv of abyssal upwelling at $\sigma_2 \approx 1037.053$. Volume tendency due to salinity trends also contribute to the densification in the Indo-Pacific, peaking at −6.5 Sv at $\sigma_2 \approx 1037.035$ and corresponding to a basin-averaged increase in salinity of around 0.001 psu over the ECCO period.

The deep Southern Ocean is warming and salinifying in ECCO. The trends have partially compensating effects on the density and hence the isopycnal volume budget. Temperature-driven isopycnal deepening peaks at 12.9 Sv at $\sigma_2 \approx 1037.157$ and is associated with a basin-averaged warming of around 0.03 C° over the ECCO period, while salinity-driven isopycnal shoaling peaks at −11.88 Sv at $\sigma_2 \approx 1037.16$, corresponding to a basin-averaged salinity increase of around 0.001 psu over the ECCO period. Note that the salinity trend below $\sigma_2 = 1037.18$ kg/m^3 appears to be primarily associated with the salt plume forcing (Figure 4).

4. Summary and Discussion

ECCO supports an interconnected view of the MOC (summarized in Figure 6), with substantial linkages between the AMOC and the abyssal cell. It is clear that substantial diapycnal upwelling (or isopycnal rising) in the Indo-Pacific is needed to balance the inflow of dense NADW into the Southern Ocean. We also find significant up- and down-welling within the Atlantic, the latter of which is not typically included in idealized depictions of the mid-depth cell.

In both the Indo-Pacific and Atlantic ocean basins, much of the net up- and down-welling is primarily balanced by isopycnal volume changes, rather than mixing-driven watermass transformations as usually assumed in theoretical models. The associated isopycnal depth trends in ECCOv4r4 represent vertical isopycnal displacement velocities on the order of 5–20 m/yr and persist over the entire ECCO period (Figures 7a and 7c). These trends are present in all of the major ocean basins and are relatively horizontally homogeneous over the Atlantic and Indo-Pacific basins (Figures 7b and 7d).

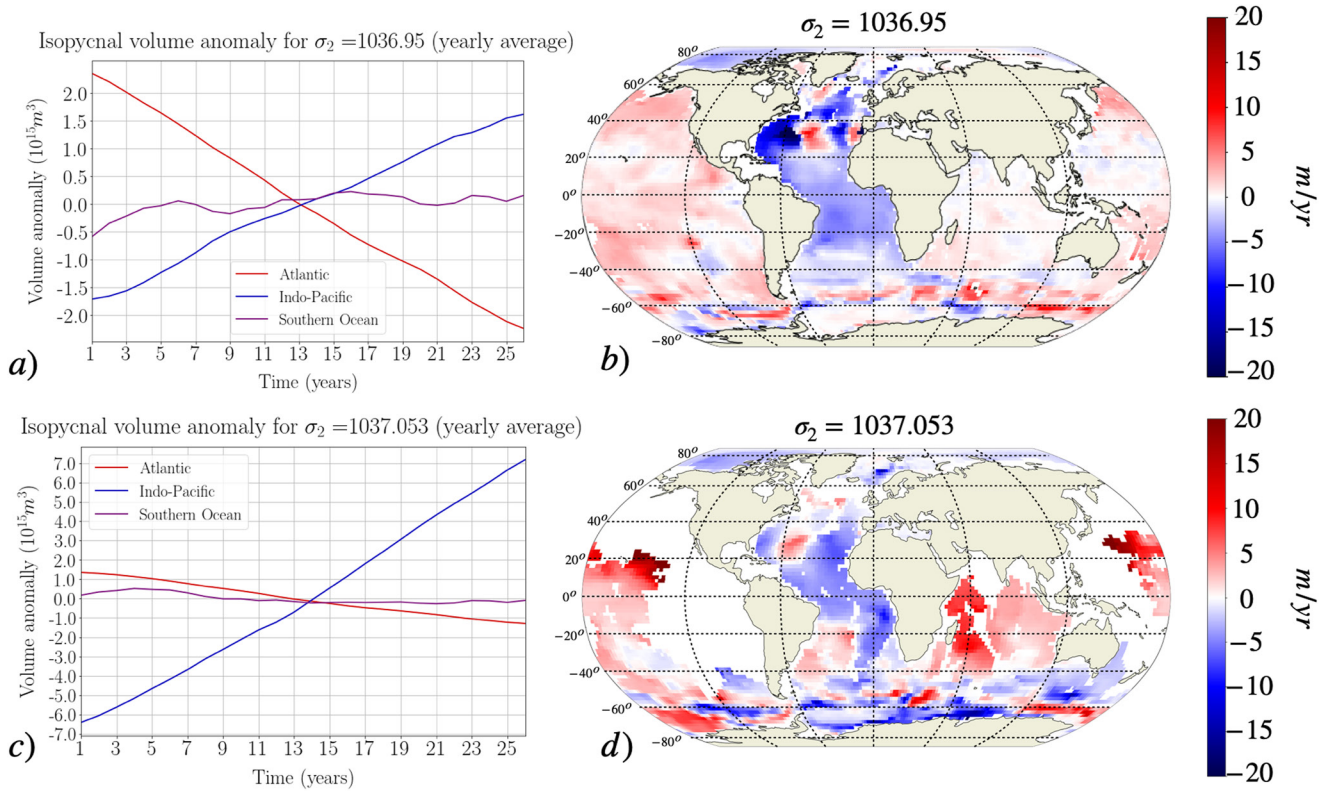

Figure 7. Trends in overall isopycnal volumes as calculated from yearly means and subdivided by basin (a and c), and spatial fields of time-averaged vertical isopycnal velocities, in meters per year, (b and d) for σ_2 = 1036.95 kg/m^3 (top) and σ_2 = 1037.053 kg/m^3 (bottom) over the Estimating the Circulation and Climate of the Ocean version 4 release 4 (1992–2017).

In the Atlantic, we find deepening mid-depth isopycnals and an overall lightening of the deep ocean associated with warming temperatures and decreasing salinity (Figures 5a and 5d). A warming deep Atlantic is broadly consistent with other reanalysis products (Palmer et al., 2015), observations (Desbruyères et al., 2017), and Green's function analysis (Gebbie & Huybers, 2019; Messias & Mercier, 2022; Zanna et al., 2019), although these studies share some of the same data sources as ECCOv4r4 and are accompanied by large uncertainties. It is also possible that an under-representation of dense water inflows across the GIS ridges in ECCOv4r4 may lead to biases in deep Atlantic density trends by limiting the amount of dense water entering the Atlantic basin (Lee et al. (2019); Lumpkin and Speer (2007); Rossby et al. (2018); Tesdal and Haine (2020)).

In the Indo-Pacific, meanwhile, we see isopycnal shoaling primarily associated with a cooling of the abyssal ocean (Figures 5b, 5e c.f. Wunsch and Heimbach (2014), Liang et al. (2015)). A cooling abyssal Indo-Pacific is consistent with Gebbie and Huybers (2019), but is in disagreement with Purkey and Johnson (2010) who suggest a broad warming in the region. The isopycnal shoaling in ECCO is a leading order term in the abyssal isopycnal volume budget in ECCO, where abyssal upwelling is balanced primarily by isopycnal shoaling as opposed to diapycnal mixing, as usually assumed in equilbrium theories such as Munk (1966) or Nikurashin and Vallis (2011). Unfortunately, as argued by Wunsch and Heimbach (2014), it is impossible to be sure whether these trends are the result of long-term trends in ocean climate, intrinsic ocean variability, or modeling and/or sampling biases, given the large uncertainties and sparseness of measurements in the deep ocean. However, it is plausible that isopycnal shoaling in ECCO's deep Indo-Pacific is due to an underrepresentation of diapycnal diffusivities in ECCO. A recent study by Trossman et al. (2022) showed that ECCO's representation of diapycnal mixing in the deep ocean is much smaller than the mixing rates suggested by microstructure measurements (Waterhouse et al., 2014) and estimates of mixing from internal wave breaking (de Lavergne et al., 2016).

Numerical diapycnal diffusion also apears to play a significant role in the volume budget of all basins and is especially prevalent in ECCO's abyssal Indo-Pacific (Figure 4b). The presence of numerical diffusion in ECCO is not surprising, as nonphysical numerical diffusion is an inherent property of depth-coordinate circulation

models (Griffies et al., 2000), and previous studies have shown that it can be large enough to exceed the rate of explicit mixing (Lee et al., 2002; Megann, 2017; Urakawa & Hasumi, 2014). In addition, the slope clipping invoked in ECCO's isopycnal mixing scheme is likely to have a significant effect on diapycnal mixing in the Southern Ocean. These spurious sources of diapycnal mixing should be taken into consideration in future model development.

The prominence of the volume tendency term in ECCO's deep ocean watermass transformation budget must be accounted for when interpreting ECCO's representation of the overturning circulation. In the equilibrium view, deep water formation in the high latitudes must be balanced by either wind-driven upwelling along isopycnals or irreversible processes in the ocean interior, which are typically assumed to be dominated by diapycnal mixing (e.g., Ferrari et al., 2017; Marshall & Speer, 2012; Munk, 1966; Nikurashin & Vallis, 2011; Wunsch & Ferrari, 2004). Such a balance does not hold in the deep ocean of ECCOv4r4 –not even to zeroth order; instead, the model depicts a global ocean where much of the apparent diapycnal up- and down-welling is balanced primarily by transient volume tendencies associated with warming (Atlantic), cooling (Indo-Pacific), and both (the deep Southern Ocean).

If the ECCO solution is correct, theories of a primarily mixing-driven abyssal overturning circulation in equilibrium with bottom water production rates cannot be applied to the present-day ocean. However, there is evidence that suggests at least some of the trends in ECCO may be the result of biases in the representation of watermass transformation processes. Stronger observational constraints are needed in order to test the validity of these trends and to reconcile the ECCOs small abyssal mixing rates with modern observations.

Whether or not the ECCO solution is correct, the presence of isopycnal volume trends needs to be considered when interpreting ECCO's climatological mean state, as the assumption of an equilibrium state leads to apparent interior watermass transformations that are actually associated with trends in the watermass volumes. For example, a recent study by Zhai et al. (2021) observed the apparent "densification" (i.e., downwelling) of NADW as it traveled southwards through the Atlantic in ECCO's climatological mean, which they speculated was the result of diapycnal mixing. Our results instead suggest that this downwelling is indeed largely adiabatic and balanced by a density trend.

Appendix A

A1. Estimating Watermass Transformation Due To Numerical Diffusion

Here we present a method for estimating the contribution of numerical diffusion to the isopycnal volume budget by treating it as the residual between the advective transport inferred from the volume budget and that inferred from the temperature and salinity tendencies provided by ECCO's advection scheme.

First, we note that the net horizontal transport beneath an isopycnal, $\Delta\Psi$, can be directly related to the advective density tendency on the bounding isopycnal. Consider an isopycnal volume, V, of ocean bounded by meridional walls in the zonal, latitudes y_1 and y_2 in the meridional, and the seafloor and the depth of the σ_2 isopycnal surface in the vertical. For a Boussinesq fluid, conservation of volume implies there is no net advective transport across the volume's boundaries and thus:

$$\Psi(y_2,\sigma_2)-\Psi(y_1,\sigma_2)+\iint_{S(y_1,y_2,\sigma_2,t)}\mathbf{v}\cdot\hat{\eta}\,dS=0, \tag{A1}$$

where $S(y_1, y_2, \sigma_2, t)$ is the isopycnal surface bounding the volume at the top, and $\hat{\eta}=\nabla\sigma_2/|\nabla\sigma_2|$ is the unit vector normal to the isopycnal surface. Using that $dS=|\nabla\sigma_2|/|\partial_z\sigma_2|dA$, where dA is the projected horizontal area of the isopycnal surface element dS, we find:

$$\begin{aligned}\Delta\Psi=\Psi(y_2,\sigma_2)-\Psi(y_1,\sigma_2)&=-\iint_{S(y_1,y_2,\sigma_2,t)}\mathbf{v}\cdot\frac{\nabla\sigma_2}{|\partial_z\sigma_2|}\,dA\\&=-\iint_{S(y_1,y_2,\sigma_2,t)}\frac{1}{|\partial_z\sigma_2|}\left(\mathbf{v}\cdot\frac{\partial\sigma_2}{\partial\theta}\nabla\theta+\mathbf{v}\cdot\frac{\partial\sigma_2}{\partial S}\nabla S\right)dA\\&=\frac{\partial}{\partial\sigma_2}\iiint_{V(y_1,y_2,\sigma_2,t)}\frac{\partial\sigma_2}{\partial\theta}\mathbf{v}\cdot\nabla\theta+\frac{\partial\sigma_2}{\partial S}\mathbf{v}\cdot\nabla S\,dV.\end{aligned} \tag{A2}$$

We now express the temperature and salinity tendencies due to the numerical advection sheme in the model, $\dot{\theta}_{adv}$ and $\dot{S}_{adv}$ (which can be computed from the ECCO output—see Piecuch (2017)), as the sum of the true tendencies and an error that includes the numerical diffusion; that is, $\dot{\theta}_{adv} = -\mathbf{v}\cdot\nabla\theta + \dot{\theta}_{num}$ and $\dot{S}_{adv} = -\mathbf{v}\cdot\nabla S + \dot{S}_{num}$. Defining the associated watermass conservation rates as

$$T_{adv} = \frac{\partial}{\partial\sigma_2}\iiint_{V(y_1,y_2,\sigma_2,t)} \frac{\partial\sigma_2}{\partial\theta}\dot{\theta}_{adv} + \frac{\partial\sigma_2}{\partial S}\dot{S}_{adv}\, dV, \tag{A3}$$

and

$$T_{num} = \frac{\partial}{\partial\sigma_2}\iiint_{V(y_1,y_2,\sigma_2,t)} \frac{\partial\sigma_2}{\partial\theta}\dot{\theta}_{num} + \frac{\partial\sigma_2}{\partial S}\dot{S}_{num}\, dV, \tag{A4}$$

and using Equation A2, we find:

$$T_{num}(y_1, y_2, \sigma_2, t) = \Delta\Psi(y_1, y_2, \sigma_2, t) + T_{adv}(y_1, y_2, \sigma_2, t). \tag{A5}$$

Data Availability Statement

The ECCO data are publicly available at https://ecco-group.org/products.htm. The analysis presented in this manuscript was done partly using the ECCOv4-py software package (https://ecco-v4-python-tutorial.readthedocs.io) under the MIT License and xarray (Hoyer & Hamman, 2017) (https://docs.xarray.dev/en/stable/) under the Apache Licesnse 2.0. Figures are plotted using the Python Package Matlplotlib 3.3.2 (Hunter, 2007), available under the Matplotlib license at https://zenodo.org/record/7527665#.Y8Gpqy2B30o. Additional analysis is done using the xmitgcm package (https://github.com/MITgcm/xmitgcm) under the MIT License. The equation of state calculation was done using the fastjmd95 python package https://zenodo.org/record/4498376#.Y8Gyoi2B30o, available as part of the xgcm package under the MIT License. Analysis scripts employed in this manuscript are publicly available at https://zenodo.org/record/7535840#.Y8H3Ei2B30o (Monkman, 2023).

Acknowledgments
This work was supported by the National Science Foundation through award OCE-1846821. The authors would like to thank Paola Cessi for providing her MATLAB scripts for the ECCO data analysis for comparison, and two anonymous reviewers for their helpful comments.

References

Abernathey, R. P., Cerovecki, I., Holland, P. R., Newsom, E., Mazloff, M., & Talley, L. D. (2016). Water-mass transformation by sea ice in the upper branch of the southern ocean overturning. *Nature Geoscience*, *9*(8), 596–601. https://doi.org/10.1038/NGEO2749

Cessi, P. (2019). The global overturning circulation. *Annual Review of Marine Science*, *11*(1), 249–270. https://doi.org/10.1146/annurev-marine-010318-095241

de Lavergne, C., Groeskamp, S., Zika, J., & Johnson, H. (2022). The role of mixing in the large-scale ocean circulation. *Ocean Mixing*, 35–63. https://doi.org/10.1016/b978-0-12-821512-8.00010-4

de Lavergne, C., Madec, G., Le Sommer, J., George Nurser, A. J., & Naveira Garabato, A. (2016). On the consumption of Antarctic Bottom Water in the abyssal ocean. *Journal of Physical Oceanography*, *46*(2), 635–661. https://doi.org/10.1175/JPO-D-14-0201.1

Desbruyères, D. G., McDonagh, E. L., King, B. A., & Thierry, V. (2017). Global and full-depth ocean temperature trends during the early twenty-first century from Argo and repeat hydrography. *Journal of Climate*, *30*(6), 1985–1997. https://doi.org/10.1002/2015GL067254

ECCO Consortium, Fukumori, I., Wang, O., Fenty, I., Forget, G., Heimbach, P., & Ponte, R. M. (2021). Synopsis of the ECCO central production global ocean and sea-ice state estimate (version 4 release 4). *ECCO Consortium*. https://doi.org/10.5281/zenodo.4533349

ECCO Consortium, Fukumori, I., Wang, O., Fenty, I., Forget, G., Heimbach, P., & Ponte, R. M. (2022). *ECCO central estimate (version 4 release 4)*. ECCO Consortium. Retrieved from https://ecco.jpl.nasa.gov/drive/files/Version4/Release4/

Ferrari, R., & Ferreira, D. (2011). What processes drive the ocean heat transport? *Ocean Modelling*, *38*(3–4), 171–186. https://doi.org/10.1016/j.ocemod.2011.02.013

Ferrari, R., Jansen, M., Adkins, J., Burke, A., Stewart, A., & Thompson, A. (2014). Antarctic sea ice control on ocean circulation in present and glacial climates. *Proceedings of the National Academy of Sciences*, *111*(24), 8753–8758. https://doi.org/10.1073/pnas.1323922111

Ferrari, R., Nadeau, L., Marshall, D. P., Allison, L. C., & Johnson, H. L. (2017). A model of the ocean circulation with two closed basins and a reentrant channel. *Journal of Physical Oceanography*, *47*(12), 2887–2906. https://doi.org/10.1175/JPO-D-16-0223.1

Forget, G. A. E. L., Campin, J. M., Heimbach, P., Hill, C. N., Ponte, R. M., & Wunsch, C. (2015). ECCO version 4: An integrated framework for non-linear inverse modeling and global ocean state estimation. *Geoscientific Model Development*, *8*(10), 3071–3104. https://doi.org/10.5194/gmd-8-3071-2015

Forget, G., & Ponte, R. (2015). The partition of regional sea level variability. *Progress in Oceanography*, *137*, 173–195. https://doi.org/10.1016/j.pocean.2015.06.002

Ganachaud, A., & Wunsch, C. (2000). Improved estimates of global ocean circulation, heat transport and mixing from hydrographic data transport. *Nature*, *408*, 408–453. https://doi.org/10.1038/35044048

Gaspar, P., Grégoris, Y., & Lefevre, J.-M. (1990). A simple eddy kinetic energy model for simulations of the oceanic vertical mixing: Tests at station Papa and long-term upper ocean study site. *Journal of Geophysical Research*, *95*(C9), 16179–16193. https://doi.org/10.1029/JC095iC09p16179

Gebbie, G., & Huybers, P. (2019). The little ice age and the 20th-century deep Pacific cooling. *Science*, *363*(6422), 70–74. https://doi.org/10.1126/science.aar8413

Gent, P. R., & Mcwilliams, J. C. (1990). Isopycnal mixing in ocean circulation models. *Journal of Physical Oceanography*, *20*(1), 150–155. https://doi.org/10.1175/1520-0485(1990)020〈0150:IMIOCM〉2.0.CO;2

Gnanadesikan, A. (1999). A simple predictive model for the structure of the oceanic pycnocline. *Science*, *283*(5410), 2077–2079. https://doi.org/10.1126/science.283.5410.2077

Gordon, A. (2001). Bottom water formation. In *Encyclopedia of ocean sciences* (2nd ed.). https://doi.org/10.1016/B978-012374473-9.00006-0

Griffies, S. M., Pacanowski, R. C., & Hallberg, R. W. (2000). Spurious diapycnal mixing associated with advection in a z-coordinate ocean model. *Monthly Weather Review*, *128*, 538–564. https://doi.org/10.1175/1520-0493(2000)128〈0538:SDMAWA〉2.0.CO;2

Hoyer, S., & Hamman, J. (2017). xarray: N-D labeled arrays and datasets in Python. *Journal of Open Research Software*, *5*(1). 10. https://doi.org/10.5334/jors.148

Hunter, J. D. (2007). Matplotlib: A 2d graphics environment. *Computing in Science & Engineering*, *9*(3), 90–95. https://doi.org/10.1109/MCSE.2007.55

Kunze, E. (2017). The internal-wave-driven meridional overturning circulation. *Journal of Physical Oceanography*, *47*(11), 2673–2689. https://doi.org/10.1175/JPO-D-16-0142.1

Lee, M.-M., Coward, A. C., & George Nurser, A. (2002). Spurious diapycnal mixing of the deep waters in and eddy-permitting global ocean model. *Journal of Physical Oceanography*, *32*, 1522–1535. https://doi.org/10.1175/1520-0485(2002)032〈1522:SDMOTD〉2.0.CO;2

Lee, S.-K., Lumpkin, R., Baringer, M. O., Meinen, C. S., Goes, M., Dong, S., et al. (2019). Global meridional overturning circulation inferred from a data-constrained Ocean and sea-ice model. *Geophysical Research Letters*, *46*(3), 1521–1530. https://doi.org/10.1029/2018GL080940

Liang, X., Piecuch, C. G., Ponte, R. M., Forget, G., Wunsch, C., & Heimbach, P. (2017). Change of the global ocean vertical heat transport over 1993–2010. *Journal of Climate*, *30*(14), 5319–5327. https://doi.org/10.1175/JCLI-D-16-0569.1

Liang, X., Wunsch, C., Heimbach, P., & Forget, G. (2015). Vertical redistribution of oceanic heat content. *Journal of Climate*, *28*(9), 3821–3833. https://doi.org/10.1175/jcli-d-14-00550.1

Lumpkin, R., & Speer, K. (2007). Global ocean meridional overturning. *Journal of Physical Oceanography*, *37*(10), 2550–2562. https://doi.org/10.1175/JPO3130.1

Macdonald, S., Meching, A. M., Toole, J., Robbins, P., Johnson, G., Wijffels, S., et al. (2009). The WOCE-era 3-D Pacific Ocean circulation and heat budget. *Progress in Oceanography*, *82*(4), 281–325. https://doi.org/10.1016/j.pocean.2009.08.002

Marshall, J., Hill, C., Perelman, L., & Adcroft, A. (1997). Hydrostatic, quasi-hydrostatic, and nonhydrostatic Ocean modeling. *Journal of Geophysical Research*, *102*(C3), 5733–5752. https://doi.org/10.1029/96JC02776

Marshall, J., & Speer, K. (2012). Closure of the meridional overturning circulation through southern ocean upwelling. *Nature Geoscience*, *5*(3), 171–181. https://doi.org/10.1038/ngeo1391

Megann, A. (2017). Estimating the numerical diapycnal mixing in an eddy-permitting ocean model. *Ocean Modelling*, *121*, 19–33. https://doi.org/10.1016/j.ocemod.2017.11.001

Messias, M., & Mercier, H. (2022). The redistribution of anthropogenic excess heat is a key driver of warming in the North Atlantic. *Communications Earth & Environment*, *3*(1), 118. https://doi.org/10.1038/s43247-022-00443-4

Monkman, T. (2023). Jgr: Oceans ECCOv4r4 analysis. Zenodo. Retrieved from https://zenodo.org/record/7535840#.Y8H3Ei2B30o

Munk, W. H. (1966). Abyssal recipes. *Deep-Sea Research*, *13*(4), 707–730. https://doi.org/10.1016/0011-7471(66)90602-4

Nadeau, L., Ferrari, R., & Jansen, M. F. (2019). Antarctic sea ice control on the depth of North Atlantic deep water. *Journal of Climate*, *32*(9), 2537–2551. https://doi.org/10.1175/JCLI-D-18-0519.1

Newsom, E. R., Bitz, C. M., Bryan, F. O., Abernathey, R., & Gent, P. R. (2016). Southern Ocean deep circulation and heat uptake in a high-resolution climate model. *Journal of Climate*, *29*(7), 2597–2619. https://doi.org/10.1175/JCLI-D-15-0513.1

Nikurashin, M., & Vallis, G. (2011). A theory of deep stratification and overturning circulation in the ocean. *Journal of Physical Oceanography*, *41*(3), 485–502. https://doi.org/10.1175/2010JPO4529.1

Palmer, M., Roberts, C., Balmaseda, M., Chang, Y.-S., Chepurin, G., Ferry, N., et al. (2015). Ocean heat content variability and change in an ensemble of ocean reanalysis. *Climate Dynamics*, *49*(3), 909–930. https://doi.org/10.1007/s00382-015-2801-0

Piecuch, C. G. (2017). A note on practical evaluation of budgets in ecco version 4 release 3.

Purkey, S., & Johnson, G. (2010). Warming of global abyssal and deep Southern Ocean waters between the 1990s and 2000s: Contributions to global heat and sea level rise budgets. *Journal of Climate*, *23*(23), 6336–6351. https://doi.org/10.1175/2010JCLI3682.1

Redi, M. H. (1982). Oceanic isopycnal mixing by coordinate rotation. *Journal of Physical Oceanography*, *12*, 1154–1158. https://doi.org/10.1175/1520-0485(1982)012〈1154:OIMBCR〉2.0.CO;2

Rossby, T., Flagg, C., Chafik, L., Harden, B., & Søiland, H. (2018). A direct estimate of volume, heat, and freshwater exchange across the Greenland-Iceland-Faroe-Scotland ridge. *Journal of Geophysical Research: Oceans*, *123*(10), 7139–7153. https://doi.org/10.1029/2018JC014250

Rousselet, L., & Cessi, P. (2022). Diabatic transformations along the global routes of the mid-depth meridional overturning circulation. *American Meteorolgical Society*, *52*(12), 3159–3177. https://doi.org/10.1175/JPOD-21-0256.1

Rousselet, L., Cessi, P., & Forget, G. (2021). Coupling of the mid-depth and abyssal components of the global overturning circulation according to a state estimate. *Science Advances*, *7*(21). https://doi.org/10.1126/sciadv.abf5478

Talley, L. (2013). Closure of the global overturning circulation through the Indian, Pacific, and southern Oceans: Schematics and transports. *Oceanography*, *26*(1), 80–97. https://doi.org/10.5670/oceanog.2013.07

Talley, L., Reid, J., & Robbins, P. (2003). Data-based meridional overturning streamfunctions for the global ocean. *Journal of Climate*, *16*, 3213–3226. https://doi.org/10.1175/1520-0442(2003)016,3213:DMOSFT.2.0.CO;2

Tesdal, J.-E., & Haine, T. W. N. (2020). Dominant terms in the freshwater and heat budgets of the subpolar North Atlantic ocean and Nordic seas from 1992 to 2015. *Journal of Geophysical Research: Oceans*, *125*(10). https://doi.org/10.1029/2020JC016435

Toggweiler, J., Russell, J. L., & Carson, S. R. (2006). Midlatitude westerlies, atmospheric CO_2, and climate change during the ice ages. *Paleoceanography*, *21*(PA2005). https://doi.org/10.1029/2005PA001154

Trossman, D. S., Whalen, C. B., Haine, T. W. N., Waterhouse, A. F., Nguyen, A. T., Bigdeli, A., et al. (2022). Tracer and observationally derived constraints on diapycnal diffusivities in an Ocean state estimate. *Ocean Science*, *18*(3), 729–759. https://doi.org/10.5194/os-18-729-2022

Urakawa, L. S., & Hasumi, H. (2014). Effect of numerical diffusion on the water mass transformation in eddy-resolving models. *Ocean Modelling*, *74*, 22–35. https://doi.org/10.1016/j.ocemod.2013.11.003

Walin, G. (1982). On the relation between sea-surface heat flow and thermal circulation in the ocean. *Tellus*, *34*(2), 187–195. https://doi.org/10.1111/j.2153-3490.1982.tb01806.x

Waterhouse, A. F., MacKinnon, J. A., Nash, J. D., Alford, M. H., Kunze, E., Simmons, H. L., et al. (2014). Global patterns of diapycnal mixing from measurements of the turbulent dissipation rate. *Journal of Physical Oceanography*, *44*(7), 1854–1872. https://doi.org/10.1175/JPO-D-13-0104.1

Weaver, A. J., Bitz, C. M., Fanning, A. F., & Holland, M. M. (1999). Thermohaline circulation: High-latitude phenomena and the difference between the Pacific and Atlantic. *Annual Review of Earth and Planetary Sciences*, *27*(1), 231–285. https://doi.org/10.1146/annurev.earth.27.1.231

Wolfe, C. L., & Cessi, P. (2011). The adiabatic pole-to-pole overturning circulation. *Journal of Physical Oceanography*, *41*(9), 1795–1810. https://doi.org/10.1175/2011JPO4570.1

Wunsch, C., & Ferrari, R. (2004). Vertical mixing, energy, and the general circulation of the oceans. *Annual Review of Fluid Mechanics*, *36*(1), 281–314. https://doi.org/10.1146/annurev.fluid.36.050802.122121

Wunsch, C., & Heimbach, P. (2014). Bidecadal thermal changes in the abyssal ocean. *Journal of Physical Oceanography*, *44*(8), 2013–2030. https://doi.org/10.1175/JPO-D-13-096.1

Zanna, L., Khatiwala, S., Gregory, J. M., Ison, J., & Heimbach, P. (2019). Global reconstruction of historical ocean heat storage and transport. *Proceedings of the National Academy of Sciences*, *116*(4), 1126–1131. https://doi.org/10.1073/pnas.1808838115

Zhai, Y., Yang, X., Wan, J., & Zou, S. (2021). The eastern atlantic basin pathway for the export of the North Atlantic deep waters. *Geophysical Research Letters*, *48*, 24. https://doi.org/10.1029/2021GL095615